J Intell Robot Syst
DOI 10.1007/s10846-017-0531-8

Clothoids Composition Method for Smooth Path Generation of Car-Like Vehicle Navigation

Suhyeon Gim · Lounis Adouane · Sukhan Lee · Jean-Pierre Dérutin

Received: 3 September 2016 / Accepted: 15 February 2017

Abstract This paper addresses a continuous curvature path generation problem for car-like vehicle navigation. The continuous curvature path is generated by multiple clothoids composition and parametric adjustment. According to the geometric conditions of the given initial and final configurations, the path generation problem is classified into two cases and then, each problem is solved by by appropriate proposed algorithm. The solution is obtained by iterative procedure subject to geometric constraint as well as solution constraints. For computational efficiency and fast convergence in the proposed algorithms, a *minimax sharpness constraint* is proposed as the solution constraint by minimizing the maximum sharpness of the feasible solutions. After the generation of the proposed path, the resultant curvature/sharpness diagram provides a useful information about its orientation and curvature continuity along the travel length. The proposed path planning strategy, permits us to obtain online, smooth and safe path between two defined configurations while ensuring high passengers comfort (continuous curvature and transition between the different composed clothoids). The algorithmic proposals have been applied to generate continuous curvature for two cases. The first correspond to local path planning for ensuring obstacle avoidance or lane change. The second application corresponds to global path smoothing. The resultant global path path is tested on the Lyapunov-based control scheme and showed improved performance on its steering work (reduction of 41.0% than the driving based on the raw data), which permits us therefore to validate the effectiveness of the obtained global path for car-like vehicles path following.

Keywords Continuous curvature path planning · Iterative algorithm · Minimax sharpness constraint · Nonholonomic car-like vehicle · Curvature and sharpness diagram

S. Gim · S. Lee (✉)
SungKyunKwan University, Seoburo 2066, 440-746, Suwon, Korea
e-mail: lsh1@skku.edu

S. Gim · L. Adouane (✉) · J.-P. Dérutin
Institut Pascal/IMobS3, Université Clermont Auvergne, CNRS, SIGMA, 63000 Clermont-Ferrand, France
e-mail: Lounis.Adouane@uca.fr

1 Introduction

Autonomous vehicles have attracted much attention for several decades and path planning in the autonomous vehicle has been one of the most important research topics for driving performance as well as its safety. According to the scale and covering range of the path planning scheme, two kinds of planners (or planning algorithms) are categorized as global and local [1, 2].

The global path planner is based on general navigational information (usually acquired from GPS) for a vehicle (often represented as a point mass) to travel

Published online: 18 March 2017

from its initial configuration to a final configuration through the given multiple way points [3]. The global planner also uses the overall known environment's topology or grid-map [4], but it lacks specific local data for a driving vehicle, such as actual vehicle size, lanes, speed bumps, obstacles, and road boundaries. On the contrary, the local path planner uses physical scale information taken from on-board sensors, and it focuses on the short-distance range from the vehicle's current configuration to the target configuration. This planner is usually applied for lane change or obstacle avoidance. The local planner is more reactive [5–8] in the sense that it can deal with dynamic obstacles [9, 10]. A multitude of local paths are integrated to obtain the global path for navigation [11] or local path smoothing on the given global path [12].

However, if the nonholonomic constraints inherent to car-like vehicles are not taken into account, the vehicle will have difficulties in following the given path. To reduce these difficulties, various smoothing techniques for the given path have been used by such as cubic spiral, B-spline, trigonometric splines [13–15]. Dubins [16] (*Dubins* path) and Reeds-Shepp [17] (*RS* path) proposed smooth path generation methods for nonholonomic vehicles which are composed by line and arc segments and yield the shortest travel length; however, their models lack curvature continuity. To generate a smooth path for the nonholonomic car-like vehicle, the curvature continuity is a important part to be considered since it is closely related to the steering smoothness and reduction of undesirable jerk [18].

The authors in [19] proposed a continuous curvature path (*FS* path) in the absence of obstacles. The *FS* path originates from the *RS* path, but it includes clothoid having a fixed sharpness (rate of curvature) so that the vehicle dose not need to stop to reorient its front wheels. The authors in [20] proposed an infinitely differentiable smooth path that approximates *Dubins* paths with bounded curvature and sharpness. In [14], the overtaking problem was addressed using clothoidal path by approximating the rational *Bézier* curves. The study used the homothetical factor adjusted by scalable parameters and control points; however, the solution of [14] needs a large amount of calculation for the multi-dimensional linear algebraic equation to determine a number of *Bézier* control points, and it is also difficult to acquire the curvature diagram directly from the resultant path.

The authors of [21] addressed the multiple clothoids problem to satisfy two boundary configurations through rigorous mathematial analysis with analytical proofs on its solvability and solution uniqueness. However, the solution and its algorithm are not sufficient for curvature or sharpness parameter analysis. Moreover, paired clothoids require control points that must be provided manually by a human designer. One noticeable work to be referenced is the work of [22] where it presents a simple and fast path generation method with continuous curvature of minimum sharpness that is close to human driving. However, the solution is only limited to a straight lane change maneuver example.

This paper addresses a *general* solution[1] on local path generation for nonholonomic car-like vehicle, where the problem is defined by two boundary configurations with zero curvatures at both ends. The solution path is comprised of parameter-adjusted multiple clothoids. There exists a lot of literature that deals with *Continuous Curvature Path* (**CCP**); however as far as we know, there has been only few works that provides a general solution for various configurations. The proposed algorithm for parametric (or parameter-adjusted) **CCP** (**pCCP**) could be useful for generating a local path in the obstacle avoidance maneuver or smoothing a given raw noisy path. To validate the effectiveness of the proposed path solution, *Lyapunov*-based controller [23–25] was tested and evaluated on the obtained path.

The main contributions of the presented work are summarized in what follows. At first, the proposed path planning strategy, permits us to obtain online, smooth and safe path between two defined configurations while ensuring high passengers comfort, which is not precisely addressed simultaneously by the dedicated literature in this field (cf. for instance *Dubins* path, *RS* path, and *FS* path). Secondly, the proposed work has different contributions compared to previous important works such as *Dubins* path, *RS* path, and *FS* path, in fact, the proposed solution allows to use the sharpness (cf. Eq.(4)) as an adjustable parameter to determine the clothoid parameters. Contrary to that, *Dubins* and *RS* paths did not use any clothoid segment for the path since the path is only designed to obtain shortest distance and without considering thus neither orientation nor curvature continuities. At third, the *FS*

[1]The solution covers various boundary configurations as much as possible by general iterative procedure.

path tackles the problem of zero curvatures at both boundary configurations (*line-to-line*) by applying a fixed value of sharpness in symmetric clothoids paths.

In the following sections, the property of parametric clothoids and its variation rules are addressed to propose the **pCCP** (cf. Section 2) with problem definition and its solution algorithms (cf. Sections 3 to 5). The different proposals are applied to several demonstrative examples (cf. Section 5).

2 Parametric Clothoid and Convergence Property

Nonholonomic car-like vehicle is driven by acceleration/brake actuation at rear and/or front wheels, while it is steered always by the front wheels. The vehicle motion is presented by *nonholonomic* kinematics equations where it is assumed that there exists no rolling contact-slip on the ground surface with tyres and thus, the steering angle corresponds to the curvature at the vehicle's motion center. When the vehicle is modeled as a point of the motion center, the nonholonomic vehicle kinematics are represented by following differential form.

$$\dot{x}\left(t\right)=v\left(t\right)\cdot cos\theta\left(t\right) \tag{1}$$

$$\dot{y}\left(t\right)=v\left(t\right)\cdot sin\theta\left(t\right) \tag{2}$$

$$\dot{\theta}\left(t\right)=\frac{v\left(t\right)}{L}\cdot tan\gamma\left(t\right) \tag{3}$$

where, $v\left(t\right)$ and $\theta\left(t\right)$ are the linear velocity and orientation angle at time t respectively and $x\left(t\right)$, $y\left(t\right)$ ($x\in\mathbb{R}^2$, $y\in\mathbb{R}^2$) represent the position of the vehicle, i.e., middle position of rear wheels. $\gamma\left(t\right)$ is the steering angle of the vehicle at time t and it is equal to the curvature $\kappa\left(t\right)$ where the radius of curvature $\rho\left(t\right)$ is defined by the two axis interconnection at the *Instantaneous Center of Rotation* (ICR) and L is the wheel base.

To describe the vehicle's path in considered time, the steering angle data at all the time are required with given initial pose. However, in the path generation problem of connecting the initial to final position, the steering data should be found only from the both end positions by implementing computational method. One possible method to obtain a solution is to adopt *try-and-error* or iterative procedure with appropriate parameters variation and constraints in order to guarantee the solution convergence [26–28]. Here, 1^{st} order clothoid (or *Euler* spiral, cf. Eq.(4)) is used as a basic component in the path and each segment is composed with other clothoid to generate the solution path under the constraint of using the minimum number of clothoid segments (CCP problem). A CCP can be simply and efficiently represented using *clothoids*. A path defined with clothoids is efficient for analyzing and controlling a car-like vehicle. In fact, this kind of path provides straightforward information on the progress of the curvature along the length and provide thus quasi immediate maneuvering information to the vehicle control system.

Using the definition of clothoid [21], the coordinates x, y are consecutively defined along the length s. If a basic formulation for clothoid curvature $\kappa(s)$ is assumed using a simple first-order polynomial with initially zero, the path is determined by integration procedures with length variable s as follows;

$$\kappa\left(s\right)=\alpha s \tag{4}$$

$$\theta\left(s\right)=\int_0^s\kappa\left(u\right)du \tag{5}$$

$$x\left(s\right)=\int_0^s\cos\theta\left(u\right)du \tag{6}$$

$$y\left(s\right)=\int_0^s\sin\theta\left(u\right)du \tag{7}$$

where α is the sharpness and $\kappa\left(s\right)$ is the curvature.

Equation 4 determines if the curvature increases or decreases by constant sharpness α, and the orientation θ in Eq. 5 changes with the integration of curvature by s in Eq. 4.

When a clothoid is generated from Eqs.(4) to (7), the parameter values at the end point have following relations with each other.

$$\kappa=\sqrt{2\delta\alpha}\left(or\delta=\frac{\kappa^2}{2\alpha}\right),s=\sqrt{\frac{2\delta}{\alpha}} \tag{8}$$

where α, δ, and κ are the values at the end points of the clothoid, and the parameter δ is the amount of orientation change between both ends (*deflection*, >0), also described in [18, 22].

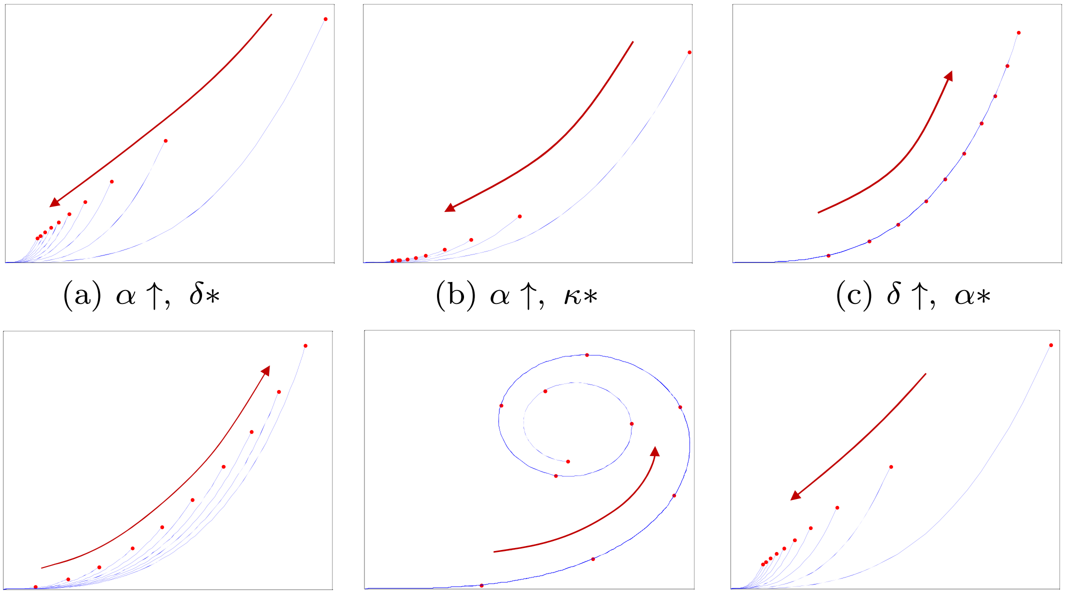

Fig. 1 Basic properties on a clothoid parameters variation

In fact, the exact *Cartesian* position at the clothoid end is difficult to determine without full integration along the travel length (cf. Eqs.(4) to (7)) or without any approximated functions (cf. [22]), however the pattern for the end point variation of the clothoid could be derived from the above parametric relations. As the parameter varies, the shape and end point of the clothoid also varies, where the following patterns are observed as shown in Fig. 1.

From the observed patterns in Fig. 1, the geometric properties are summarized as follows.

Property 1 [Clothoid geometric property on parameter variation] Among the three clothoid parameters (α, δ, and κ),

i. As the sharpness α increases with another parameter constant, the clothoid shrinks (cf. Fig. 1a and b).

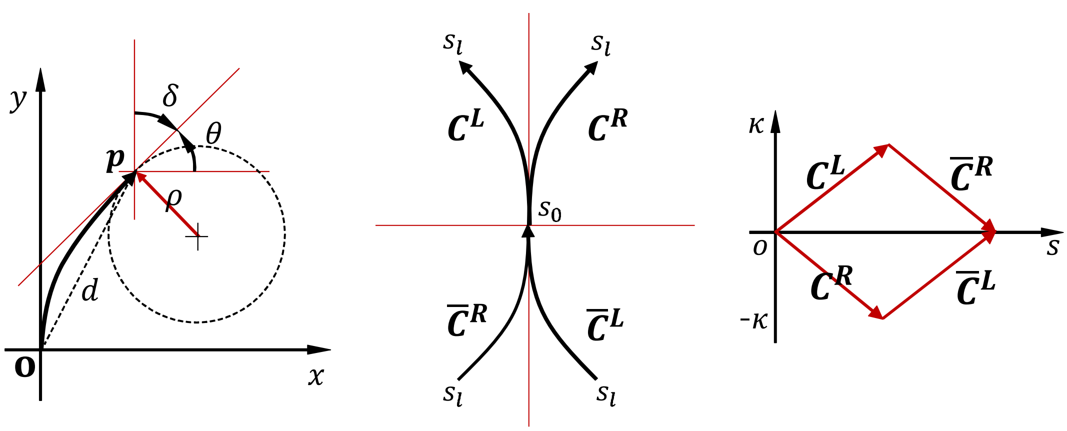

Fig. 2 Notation and Convention on an elementary clothoid generation

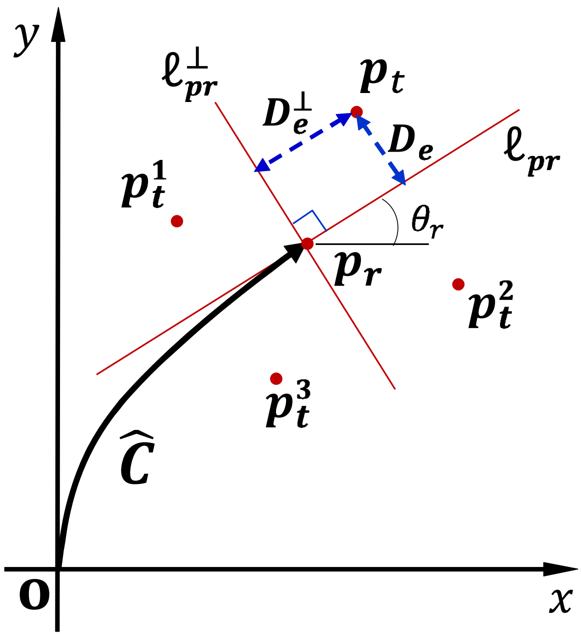

Fig. 3 D_e definition for convergence criteria

ii. As the deflection δ increases with another parameter constant, the clothoid expands (cf. Fig. 1c and d).

iii. As the curvature κ increases with δ constant, the clothoid shrinks (cf. Fig. 1f).

Using the properties, multiple clothoids are composed by parametric adjuatment. Before entering into the problem definition and its solution, it is required to mention about some conventions and notions for the composition method.

Property 2 [Notation for curvature positivity] A clothoid is generated so that its length s increases from zero s_0 through its length s_l, i.e., as $s \rightarrow [s_0, s_l]$, $\boldsymbol{C} \rightarrow [\boldsymbol{C}(s_0), \boldsymbol{C}(s_l)]$. The $\kappa(s)$ is positive when the vehicle steering angle is in the left hand side from its center and negative for the right hand side. Also, $\alpha(s)$ is positive when the vehicle turns counter-clockwise, as $\boldsymbol{C}^{\boldsymbol{L}}$, and negative for clockwise rotation as $\boldsymbol{C}^{\boldsymbol{R}}$. The $\theta(s)$ is obtained by integration of curvature by clockwise direction on the *Cartesian* coordinate, and the δ is calculated by the orientation changes from initial to final pose, thus $\delta > 0$ for $s \rightarrow [s_0, s_l]$. These geometric patterns could be obtained by mathematical analogy, and described in Appendix.

Property 3 [Clothoids composition] To compose $\boldsymbol{C_1}$ and $\boldsymbol{C_2}$ with geometric continuities (orientation G^1 and curvature G^2), the operator $\oplus$ is used (i.e., $\boldsymbol{C_1} \oplus \boldsymbol{C_2}$). If one is $\boldsymbol{C}^{\boldsymbol{R}} = \boldsymbol{C_1}$, then the other is $\boldsymbol{C_2} = \bar{\boldsymbol{C}}^{\boldsymbol{L}}$, or vice versa., where the superscript $\boldsymbol{R}$, $\boldsymbol{L}$ stand for *right*, *left* turning respectively, and $\bar{\boldsymbol{C}}$ presents the reverse form of $\boldsymbol{C}$ which is generated from the final to the initial by $s \rightarrow [s_l, s_0]$.

Here, we define an *elementary* clothoid that its initial curvature is zero and its deflection is below $\frac{\pi}{2}$. Figure 2 describes about parameters notations and its shape convention for an elementary clothoid.

In Fig. 2a, the clothoid is generated from $\mathbf{o}$ to $\boldsymbol{p}$ point (the shortest distance d), where orientation θ and deflection δ (cf. orientation difference between initial and final positions) are denoted. The radius of curvature ρ is shown with a tangential circle at $\boldsymbol{p}$, which presents the curvature of $\frac{1}{\rho}$. Figure 2b and c depict the clothoid

Fig. 4 Case A ($\boldsymbol{C}_1^{\boldsymbol{R}}\bar{\boldsymbol{C}}_2^{\boldsymbol{L}}$)

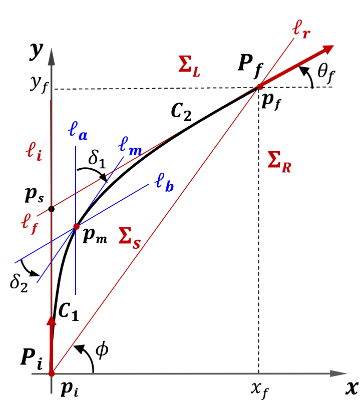

(a) Geometric representation

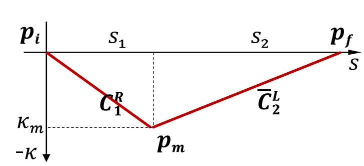

(b) Curvature diagram

path and shape conventions as noted in Property 2 and 3, respectively. The arrow of (b) indicates the path generating direction, and each clothoid is generated from s_0 to s_l. The corresponding curvature can be matched in the curvature diagram shown in Fig. 2c (with negative y axis notation, i.e., $\kappa < 0$ in $y > 0$ axis), where a clothoid is generated, then the next clothoid should be its reverse form like $\boldsymbol{C_1^R \bar{C}_2^L}$ or $\boldsymbol{C_1^L \bar{C}_2^R}$.

Another important property is the convergence and parameter variation criteria used in the iterative algorithm. Figure 3 depicts a geometric representation for convergence criteria by the clothoid parameter variation. A composed clothoid $\widehat{\boldsymbol{C}}$ by $\boldsymbol{C_1^R} \oplus \boldsymbol{\bar{C}_2^L}$ is generated to make its end point, (a reference point) $\boldsymbol{p_r}$ with the boundary condition of $\kappa_r = 0$ and $\theta_r = \theta_1$. The objective of the algorithmic loop is to determine the parameter variation rule for $\boldsymbol{p_r}$ to reach a target position, $\boldsymbol{p_t}$. For that purpose, two reference lines are defined as $\ell_{p_r}, \ell_{p_r^\perp}$ which are drawn from $\boldsymbol{p_r}$ with tangential and perpendicular direction respectively. Then, the convergence criteria are defined as,

$$|\boldsymbol{D_e}| < \varepsilon, \boldsymbol{D_e^\perp} > 0 \tag{9}$$

where $\boldsymbol{D_e}$ and $\boldsymbol{D_e^\perp}$ are the minimum distance from $\boldsymbol{p_t}$ to ℓ_{p_r} and $\ell_{p_r}^\perp$, respectively. The ℓ_{p_r} is a tangential line passing through $\boldsymbol{p_r}$ of having slope $\tan\theta_1$ and the $\ell_{p_r}^\perp$ is the perpendicular line to ℓ_{p_r} while passing $\boldsymbol{p_r}$. The criteria in Eq. 9 indicate that the convergence is passed if the absolute distance error $|\boldsymbol{D_e}|$ is less than a designed threshold ε while holding a positive value for $\boldsymbol{D_e^\perp}$. Here, the condition $\boldsymbol{D_e^\perp} \geq 0$ allows the inclusion of a line segment to complete the path solution by connecting $\boldsymbol{p_r}$ to $\boldsymbol{p_t}$ after the condition of $|\boldsymbol{D_e}| \leq \varepsilon$ is satisfied.

The parameter variation in the algorithmic loop is based on the geometric relation between ℓ_{p_r} and $\boldsymbol{p_t}$, as well as that between $\ell_{p_r}^\perp$ and $\boldsymbol{p_t}$. The determinant function $\lambda_{\boldsymbol{p_r}}(\boldsymbol{p_t})$, which checks the geometric relation between a target point ($\boldsymbol{p_t}$) and a reference point $\boldsymbol{p_r}$,[2] can be used to change clothoid parameter by using one of the following rule.

Remark 1 Parameter variation rule

a. If $\lambda_{\boldsymbol{p_r}}(\boldsymbol{p_t}) > 0$ (< 0), then $\boldsymbol{\alpha}$ should decrease (increase) with constant $\boldsymbol{\kappa}$,
b. If $\lambda_{\boldsymbol{p_r}}(\boldsymbol{p_t}) > 0$ (< 0), then $\boldsymbol{\delta}$ should increase (decrease) with constant $\boldsymbol{\kappa}$,
c. If $\lambda_{\boldsymbol{p_r}}(\boldsymbol{p_t}) > 0$ (< 0), then $\boldsymbol{\alpha}$ should decrease (increase) with constant $\boldsymbol{\delta}$.

Using one of rules in *Remark*, for example, $\boldsymbol{p_t}$ and $\boldsymbol{p_t^1}$ let α decrease whereas $\boldsymbol{p_t^2}$ and $\boldsymbol{p_t^3}$ allow α to increase. This Remark 1 and Eqs. 9 are utilized to adjust clothoid parameters in each iterative loop to converge to the solution, and is described in each algorithm of the next section.

3 Problem Definition and pCCP Solution

For CCP generation, multiple clothoids are composed to satisfy the boundary configuration. The initial configuration corresponds to the vehicle's local coordinate at which the local path generation begins with the vehicle oriented toward the *y-axis*. The final configuration is specified in the first quadrant plane, i.e., $x > 0$, $y > 0$ while maintaining its general solvability with symmetric compatibility. The **pCCP** problem is defiend as follows:

Problem 1 From $\boldsymbol{P_i}\left(x_i, y_i, \theta_i = \frac{\pi}{2}, \kappa_i = 0\right)$ to $\boldsymbol{P_f}\left(x_f, y_f, \theta_f, \kappa_f = 0\right)$, find a path composed of the minimum number of elementary clothoids that satisfies both configurations with curvature continuity along the length.

When ϕ is defined as the angle between $\boldsymbol{p_i}$ and $\boldsymbol{p_f}$, then according to the condition between θ_f and the reference line ℓ_r (cf. Fig. 5a) (whether $\theta_f > \phi$ or $\theta_f < \phi$), the minimum number of clothoids satisfying both configurations is either two or four. Hence, **Problem** is decomposed into two subcases **A, B** in the following two subsections.

3.1 Case A ($\theta_f < \phi$)

In this case, two clothoids are sufficient to construct the feasible path. A clothoid $\boldsymbol{C_1}$ with the shape $\boldsymbol{C^R}$, and the other clothoid $\boldsymbol{C_2}$ with $\boldsymbol{C^L}$ (cf. Property 2), compose $\widehat{\boldsymbol{C}}$ by $\boldsymbol{C_1^R} \oplus \boldsymbol{\bar{C}_2^L}$ while holding G^1 and G^2.

Figure 4 depicts the case $\theta_f < \phi$. In Fig. 4a, two extension lines from both configurations are denoted as ℓ_i, ℓ_f, respectively and ℓ_r is drawn by connecting

[2] $\lambda_{\boldsymbol{p_r}}(\boldsymbol{p_t}) = -\tan(\theta_r)\cdot x_t + \tan(\theta_r)\cdot x_r + y_t - y_r$, where $p_r(x_r, y_r)$ and $p_t(x_t, y_t)$.

$\boldsymbol{P_i}$ with $\boldsymbol{P_f}$. When three intersection points $\boldsymbol{p_i}$, $\boldsymbol{p_f}$, and $\boldsymbol{p_s}$ are defined by ℓ_i, ℓ_f, and ℓ_r respectively ($\boldsymbol{p_s}$ by ℓ_i and ℓ_f), then the areas $\boldsymbol{\Sigma_R}$, $\boldsymbol{\Sigma_L}$ are the half-space to the right and the left of ℓ_r respectively, and $\boldsymbol{\Sigma_S}$ is the area inside the polygon $\triangle \boldsymbol{p_i}\,\boldsymbol{p_f}\,\boldsymbol{p_s}$. Thus for this case, all the points in the composed clothoids are inside $\boldsymbol{\Sigma_S}$. Note that if $\theta_f = \phi$, then no clothoid pairs satisfy both configurations except a straight line since $\ell_f = \ell_r$.

Under the defined geometric representation, $\boldsymbol{C_1}$ starts from $\boldsymbol{p_i}$ to $\boldsymbol{p_m}$ (*meeting* point), while $\boldsymbol{C_2}$ starts from $\boldsymbol{p_f}$ to $\boldsymbol{p_m}$. The shape of the composed path becomes $\boldsymbol{C_1^R} \oplus \bar{\boldsymbol{C}}_{\boldsymbol{2}}^{\boldsymbol{L}}$, where $s_1 \to [s_0, s_m]$ in $\boldsymbol{C_1}$, $s_2 \to [s_m, s_f]$ in $\boldsymbol{C_2}$ from Property 3 and Fig. 4b. Note that, since $\boldsymbol{P_f}$ heads toward $\boldsymbol{\Sigma_R}$, $\boldsymbol{C_2}$ is located inside $\boldsymbol{\Sigma_L}$, and $\boldsymbol{p_m}$ also resides in $\boldsymbol{\Sigma_S}$ (cf. Property 2). The curvature of $\boldsymbol{C_1}$ grows from $\boldsymbol{p_i} = 0$ to $\boldsymbol{p_m}$ with a constant sharpness, as determined in Eq. 5, and the curvature of $\boldsymbol{C_2}$ decreases from $\boldsymbol{p_m}$ to $\boldsymbol{p_f}$. The deflections for $\boldsymbol{C_1}$ and $\boldsymbol{C_2}$ reach δ_1 and δ_2, respectively, until $\boldsymbol{p_m}$. At this point $\boldsymbol{p_m}$, there exists an important geometric constraint about G^1 constraint.

$$\delta_1 + \delta_2 = \theta_i - \theta_f. \tag{10}$$

Figure 4b depicts the corresponding curvature diagram where $\boldsymbol{C_1}$ increases its curvature to the maximum $\boldsymbol{\kappa_m}$ at $\boldsymbol{p_m}$ with G^2 continuity constraint and $\boldsymbol{C_2}$ decreases to zero at $\boldsymbol{p_f}$. About Eq. 9, Fig. 4b informs us that δ_1 is the area of the triangle for $\boldsymbol{C_1^R}$ and δ_2 is the area of the triangle for $\bar{\boldsymbol{C}}_{\boldsymbol{2}}^{\boldsymbol{L}}$, thus the sum of these two areas equals to the total deflection $\theta_i - \theta_f$.

Algorithm 1 Case A: two clothoids generation

Require: $\varepsilon, d\alpha, d\delta, \mathrm{sol} = \mathrm{FALSE}$ ▷ Pre-setting values for iterative convergence
Require: α_1, δ_1 ▷ Initial assumption
1: **procedure** CLOTHOID2LL($\boldsymbol{P_i}, \boldsymbol{P_f}$)
2: **while** sol == FALSE **do**
3: $\kappa_1 \leftarrow \alpha_1, \delta_1$ ▷ C_1 generation
4: $\kappa_2 = \kappa_1$ ▷ G^2 continuity
5: $\delta_2 \leftarrow \delta_1, \theta_f$ ▷ G^1 continuity
6: $\alpha_2 \leftarrow \kappa_2, \delta_2$ ▷ C_2 generation
7: $\widehat{C} \leftarrow C_1 \oplus C_2$ ▷ Two clothoids composition
8: $D_e \leftarrow \ell_f, \widehat{C},\ D_e^{\perp} \leftarrow \ell_f^{\perp}, \widehat{C}$ ▷ Distance error parameters
9: **if** $|D_e| < \varepsilon$ **then**
10: **if** $D_e^{\perp} \geq 0$ **then**
11: sol = TRUE ▷ Convergence achieved
12: **return** $\boldsymbol{\alpha_{sol}}, \boldsymbol{\delta_{sol}}, \widehat{\boldsymbol{C}}$ ▷ Obtained solution
13: **end if**
14: **end if**
15: $\lambda \leftarrow D_e, \lambda^{\perp} \leftarrow D_e^{\perp}$
16: **if** $\lambda \cdot \lambda' < 0$ **then** ▷ Bisection method for α
17: $d\alpha = \frac{d\alpha}{2}$
18: **end if**
19: **if** $\lambda^{\perp} \cdot \lambda'^{\perp} < 0$ **then** ▷ Bisection method for δ
20: $d\delta = \frac{d\delta}{2}$
21: **end if**
22: $d\alpha = |d\alpha| \cdot \mathrm{sign}(\lambda),\ d\delta = |d\delta| \cdot \mathrm{sign}(\lambda^{\perp})$ ▷ α, δ variation criteria
23: $\alpha_1 = (\alpha_1 + d\alpha),\ \delta_1 = (\delta_1 + d\delta)$
24: $\lambda' = \lambda,\ \lambda'^{\perp} = \lambda^{\perp}$ ▷ For next iteration
25: **end while**
26: **end procedure**

In Algorithm 1, initial values of α_1 and δ_1 for $\boldsymbol{C_1}$ are assumed before entering the loop with required pre-setting values. From the lines [3-6], the parameters to compose two clothoids are determined by geometric constraints. The parameters are adjusted from the lines [16-23] (cf. Remark 1). The parameter variation rules of lines [16-18] and lines [19-21] are same as the *bisection method* [29].[3]

[3]The bisection method guarantees the convergence.

To obtain the solution $\boldsymbol{\alpha_{sol}}, \boldsymbol{\delta_{sol}}, \widehat{\boldsymbol{C}}$, the stopping criteria are defined in line 9 and line 10, where the ε should be larger than the sampling distance of *Fresnel* integration for bisection convergence, i.e., $\varepsilon > 10^{-2}[m]$.

3.2 Case B ($\theta_f > \phi$)

The condition used to decompose the problem into two subcases is whether $\theta_f > \phi$ or not, (If $\theta_f = \phi$, only a line solution is feasible.) and this condition is determined from the geometric relation betweem $\boldsymbol{P_i}$ and $\boldsymbol{P_f}$.

Figure 5 depicts **Case B**, where the only difference from **Case A** is the orientation of $\boldsymbol{P_f}$, which is directed toward the area $\boldsymbol{\Sigma_L}$ (i.e., $\theta_f > \phi$). For this case, it is not possible to generate **pCCP** using only two clothoids; indeed, additional clothoids are required.

This condition is proved using the geometric representation as follows. In Fig. 5a, four clothoids are generated from $\boldsymbol{p_i}$ to $\boldsymbol{p_f}$ as $\boldsymbol{C_{1a}}$, $\boldsymbol{C_{1b}}$, $\boldsymbol{C_{2b}}$, and $\boldsymbol{C_{2a}}$. In the same way as for Case A, the clothoid pair $\widehat{\boldsymbol{C_1}} = \boldsymbol{C^R_{1a}} \oplus \bar{\boldsymbol{C}}^{\boldsymbol{L}}_{\boldsymbol{1b}}$, and the other pair $\widehat{\boldsymbol{C_2}} = \bar{\boldsymbol{C}}^{\boldsymbol{R}}_{\boldsymbol{2a}} \oplus \boldsymbol{C^L_{2b}}$. Each pair has the connection point $\boldsymbol{p_{m1}}$, $\boldsymbol{p_{m2}}$, and it also has common tangential line ℓ_{m1}, ℓ_{m2}, where the lines provide the reference for both clothoids deflections.

Algorithm 2 Case B: Four clothoids generation

Require: $\varepsilon, d\alpha, d\theta, \mathrm{sol} = \mathrm{FALSE}$ ▷ Pre-setting values for iterative convergence
Require: $\tan\theta_m$ ▷ Slope of ℓ_m
Require: $\alpha_1, \delta_1, \alpha_2, \delta_2$ ▷ Initial parameters assumption for C_1 and C_2
1: **procedure** CLOTHOID4LL($\boldsymbol{P_i}, \boldsymbol{P_f}$)
2: **for** $\theta_m \leftarrow (\theta_m + d\theta)$ **do**
3: **while** sol == FALSE **do**
4: **call** clothoid2LL($\boldsymbol{P_i}$, $\boldsymbol{P_m}$)
5: $\widehat{C_1} \leftarrow C_{1a} \oplus C_{1b}$
6: **call** clothoid2LL($\boldsymbol{P_f}$, $\boldsymbol{P'_m}$)
7: $\widehat{C_2} \leftarrow C_{2a} \oplus C_{2b}$
8: $D_e \leftarrow \widehat{C_1}, \widehat{C_2}$
9: $\lambda = D_e, \lambda^{\perp} = D_e^{\perp}$
10: **if** $|D_e| < \varepsilon$ **then**
11: **if** $D_e^{\perp} \geq 0$ **then**
12: sol = TRUE ▷ Convergence achieved
13: **return** $\bar{\alpha}_{sol}, \bar{\delta}_{sol}, \widehat{C}_{1,2}$ ▷ Obtained solution
14: **end if**
15: **end if**
16: **if** $\lambda \cdot \lambda' < 0$ **then** ▷ Bisection method for α_1, α_2
17: $d\alpha = \frac{d\alpha}{2}$
18: **end if**
19: **if** $\lambda^{\perp} \cdot \lambda'^{\perp} < 0$ **then** ▷ Bisection method for δ_1, δ_2
20: $d\delta = \frac{d\delta}{2}$
21: **end if**
22: $d\alpha = |d\alpha| \cdot \mathrm{sign}(\lambda)$, $d\delta = |d\delta| \cdot \mathrm{sign}(\lambda^{\perp})$ ▷ α, δ variation criteria
23: $\alpha_{1,2} = (\alpha_{1,2} + d\alpha)$, $\delta_{1,2} = (\delta_{1,2} + d\delta)$
24: $\lambda' = \lambda$, $\lambda'^{\perp} = \lambda^{\perp}$ ▷ For next iteration
25: **end while**
26: **end for**
27: **end procedure**

Under the described notations, let us assume two clothoids which connecting boundary configurations as following. If $\boldsymbol{C_{1a}}$ meets $\bar{\boldsymbol{C}}_{\boldsymbol{2a}}$, the curvature signs must be opposite to each other. If $\bar{\boldsymbol{C}}_{\boldsymbol{2a}}$ is to be the same as $\boldsymbol{C_{1a}}$, $\bar{\boldsymbol{C}}_{\boldsymbol{2a}}$ should be located outside of $\boldsymbol{\Sigma_{s2}}$ (right side of ℓ_f), which could not satisfy the orientation continuity. This result is clearly seen from the corresponding curvature diagram in Fig. 5b, $\boldsymbol{p_{m1}}$ can not meet $\boldsymbol{p_{m2}}$.

In Fig. 5b, the curvature at the first pair $\widehat{\boldsymbol{C_1}}$ produces two curvature lines of $\boldsymbol{C_{1a}}$, $\boldsymbol{C_{1b}}$, and that for the second pair $\widehat{\boldsymbol{C_2}}$ is $\boldsymbol{C_{2b}}$ and $\boldsymbol{C_{2a}}$. All curvature lines are continuously connected along the travel length, where $\widehat{\boldsymbol{C_1}}$ retains in negative curvature (upper to

Fig. 5 Case B ($\bar{C}^R_{1a}\bar{C}^L_{1b}C^L_{2b}\bar{C}^R_{2a}$)

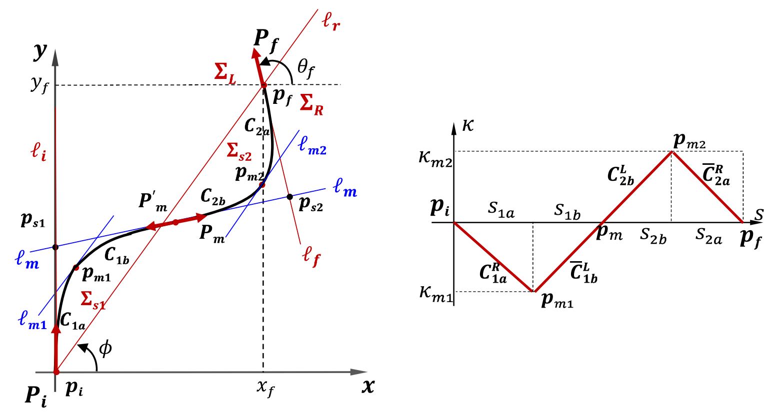

(a) Geometric representation (b) Curvature diagram

$s-axis$) and $\widehat{C_2}$ remains in the positive (under the $s-axis$).

The four clothoids composition in Case B are achieved using two consecutive pairs of **Case A** compositions. Hence, it is important to determine a common boundary condition at the intersection point of both composition pairs. To tackle this problem, a reference line ℓ_m is initially fixed at the end of the first clothoid pair $\widehat{C_1}$ with slope $\tan\theta_m$ (θ_m is the slope angle of ℓ_m). The line ℓ_m gives an orientation constraint for both $\widehat{C_1}$ and $\widehat{C_2}$. If the common orientation constraint of $\tan\theta_m$ is given, two pairs of clothoids can each be solved as two clothoid problems, according to the resolved Case A.

In Algorithm 2, two procedures are performed according to convergence criteria (lines [10-11]) using Remark 1. Note that this subcase can address two separated Case A constrained by a reference line ℓ_m which passes through $\boldsymbol{p_m}$ with the slope of $\tan\theta_m$. Furthermore, $\boldsymbol{p_m}$ and $\boldsymbol{p'_m}$ are result of the procedure **clothoid2LL** by given parameters and $\boldsymbol{p'_m}$ should be on ℓ_m with positive distance, i.e., $\boldsymbol{D^{\perp}_e} \geq 0$; This subcase has numerous solutions according to the slope of ℓ_m (cf. line 2) and the parameters of $\widehat{C}_{1,2}$; thus, additional constraint for the procedure is required. About this constraint, it is addressed specifically in Section 4.2.

4 Enhancement of Algorithmic Convergence

As the number of composed clothoids increases (which means more parameters to be defined), the algorithmic convergence time is delayed accordingly with an exponential scale. Thus, efficient constraints in the proposed algorithmic procedures have to be defined in order to obtain unique solution. The following subsections address this point based on initial parameter assumptions and a solution constraint.

4.1 Initial Parameter Assumption

Before entering into iterative procedure, both end configurations are given. Thus, α_{1i} should be tried first; however, if the generated $\boldsymbol{C_1}$ is far from the target position ($\boldsymbol{p_f}$), the procedure requires a lot of convergence time. In this respect, the method to assume an initial parameter is proposed as follows.

In the initial step, the only information from given configurations is the configuration distance (d in Fig. 3a) between the ends named by d_{if}. This means that there might be an efficient formulation linking α_{1i} to d_{if}. While being interested in the relation among the distance and clothoid parameters, the process starts from the basic property for a clothoid, as presented in Section 2. From Fig. 3a, one can observe that the distance d from the origin to clothoidal end decreases as the sharpness increases with fixed deflection.

This result reversely says the distance d_{if} increases as the sharpness decreases. Using this relation, a function that determines sharpness from the distance parameter could be approximated using a simple second-order polynomial equation[4] of $d_{\text{if}} = \mathcal{G}\alpha^2$ with $\mathcal{G}$ is a coefficient for the relation. It is also found that $\mathcal{G}$ changes with deflection δ in the clothoid; thus, δ

[4]The MATLAB function-*polyfit* was used.

needs to be included as a variable into the coefficient $\mathcal{G}$ of the approximation function as follows,

$$\begin{aligned} \alpha_{1i} &= \mathcal{G} \cdot (1/d_{\text{if}})^2, \\ \mathcal{G} &= -0.3352\delta^2 + 2.2111\delta - 0.0429 \end{aligned} \quad (11)$$

where the function approximates the relation between α_{1i} and d_{if} within 10^{-2}, where its coefficient $\mathcal{G}$ is determined using second-order polynomial fitting with the variable δ.

The derivative $d\alpha$ for the initial step can also be determined from differentiating equation (8) as $\frac{\partial \alpha_{1i}}{\partial d_{\text{if}}}$ and by inserting ∂d_{if} and current d_{if} for the given configuration, for instance using $\partial d_{\text{if}} = d_{\text{if}}/100$.

4.2 Minimax Sharpness Constraint

In the multiple clothoids problem, the proposed algorithms require additional constraint (or solution constraint) to obtain a unique solution. In this respect, as the solution constraint, *minimax sharpness constraint* (**MSC**) for two clothoids is proposed as follows.

Lemma 1 (Minimax sharpness constraint for two clothoids) *When $\widehat{C}(\alpha_1, \alpha_2)$ is a feasible solution which satisfies given two boundary conditions, maximum sharpness is described as $max[\alpha_1, \alpha_2] = \hat{\alpha}$, then the solution by* **MSC is the one of which $\hat{\alpha}$ is the minimum among the feasible solutions.**

The MSC provides a feasible solution composed two clothoids by,

$$\alpha_1 = \alpha_2, \delta_1 = \delta_2 = \frac{\theta_1 - \theta_2}{2}. \quad (12)$$

Proof When two clothoids $\boldsymbol{C_1}$ and $\boldsymbol{C_2}$ are composed as Fig. 6b, the both clothoids have a common peak curvature value (κ_c in Fig. 6c). For each clothoid in the composition, δ is varied according to α under the constraint of Eq. 8. In the graph given in Fig. 7a, let us assume that $\delta_m = \frac{\theta_1-\theta_2}{2}$.

If $\alpha_1 < \alpha_m$, then $\delta_1 > \delta_m$ by $2\delta_1\alpha_1 = C(Const.)$.

From $\delta_1 + \delta_2 = \theta_1 - \theta_2 = 2\delta_m = C'(Const.)$ by G^1 continuity at $\boldsymbol{p_c}$ of Fig. 7b, it is derived as $\delta_2 = C' - \delta_1 = 2\delta_m - \delta_1$.

Since $\delta_1 > \delta_m$, thus $\delta_2 = 2\delta_m - \delta_1 < \delta_1$ which results in $\delta_2 < \delta_1$.

It is also true that $2\delta_2 < \delta_1 + \delta_2 = 2\delta_m$, so that $\delta_2 < \delta_m$.

From $\kappa_c^2 = 2\delta_1\alpha_1 = 2\delta_2\alpha_2 = C$, it results that $\alpha_2 > \alpha_m$: $\max[\alpha_1, \alpha_2] > \alpha_m$ (**A**).

Vice versa, if $\alpha_1 > \alpha_m$, it also results that $\alpha_2 < \alpha_m$: $\max[\alpha_1, \alpha_2] > \alpha_m$ (**B**).

From above two results (**A**), (**B**), α_m is the *minimax* sharpness with the condition of $\delta_1 = \delta_2 = \frac{\theta_1-\theta_2}{2}$ and $\alpha_1 = \alpha_2$: *a symmetric pair of clothoids.* □

5 Demonstrative Examples

5.1 Local Path Planning

The proposed algorithm is applied to obtain **pCCP** for local path generation examples. The configuration in each problem is given with consideration of real vehicle size (e.g., width 1.5m and wheel base $L = 2m$) and structured road environment. In the first example, path generation for cornering-like motion and

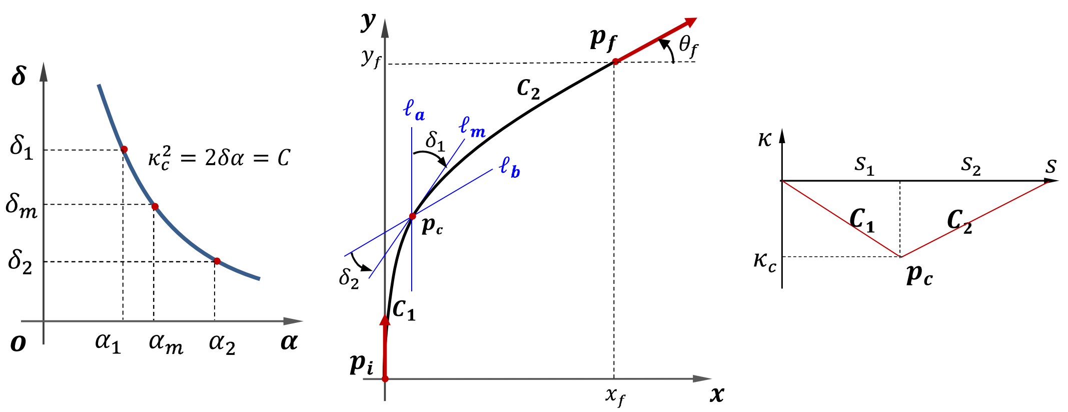

(a) $\alpha - \delta$ relation (b) Two clothoids path (c) Curvature diagram for (b)

Fig. 6 Two clothoids composition scheme

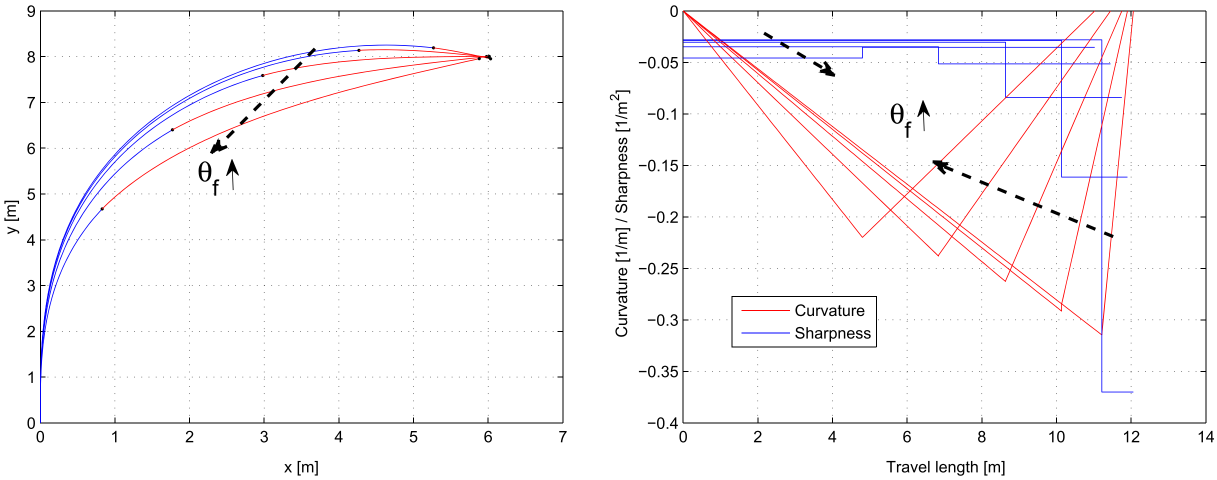

(a) Two clothoids composition

(b) C-S diagram

Fig. 7 **pCCP** for **Case A**

lane change maneuvering are carried out, where each path planning corresponds to the problem of **Case A**, **B**, respectively. For the cornering-like motion, the final configuration is given by $\boldsymbol{P_f}(6, 8, \theta_f, 0)$, and θ_f varies from $-10°$ to $30°$ per $10°$ as depicted in Fig. 7 with increasing $\theta_f \uparrow$ of a dotted arrow direction.

Figure 7 shows the two clothoids **pCCP** for **Case A**, where the obtained path and corresponding curvature-sharpness diagram (C-S diagram) are depicted. In Fig. 7b, it can be observed that, as the final orientation grows, the minimum curvature decreases from -0.22 to -0.32 as a dotted arrow direction by increasing θ_f $(\uparrow)$. For the sharpness, the peak point of curvature moves right, and the sharpness value increases as θ_f decreases. This diagram illustrates that, in vehicle driving, steering behavior becomes more difficult as the orientation difference $(\theta_i - \theta_f)$ increases.

Secondly, lane change motions are performed with a drastic lane change of 10m width (up to three lanes) with different final orientations. The final configuration is given as $\boldsymbol{P_f}(10, 12, \theta_f, 0)$, where θ_f increases $(\uparrow)$ from $70°$ to $120°$ per $10°$ for each path generation.

In Fig. 8, four clothoids **pCCP** for **Case B** is solved under the constraint of Lemma 1, constraining θ_m by

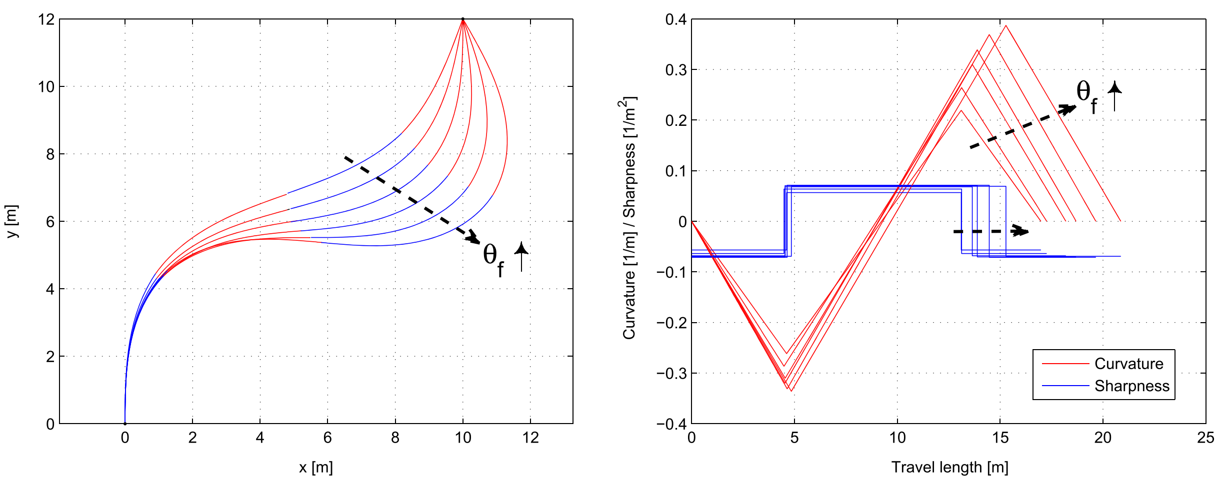

(a) Four clothoids composition

(b) C-S diagram

Fig. 8 **pCCP** for **Case B**

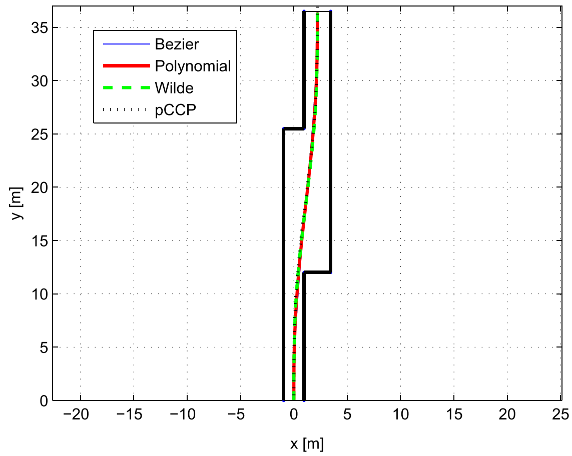

(a) Paths on equal axes

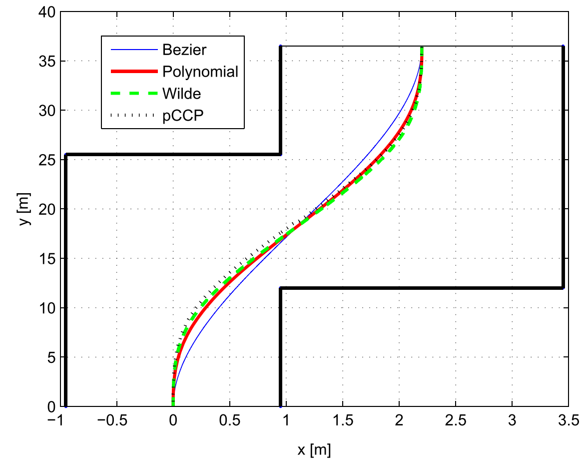

(b) Paths on normal axes

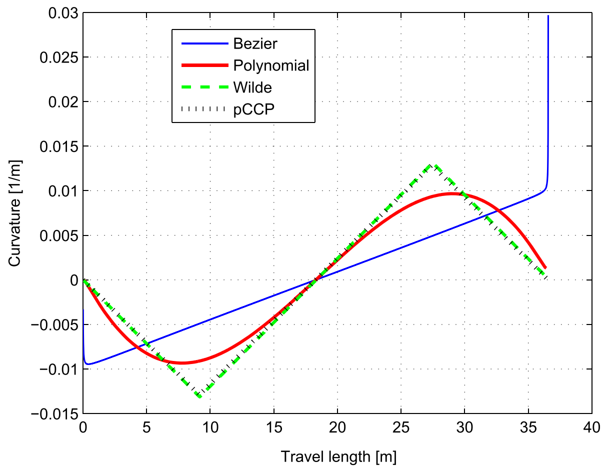

(c) Curvature diagram

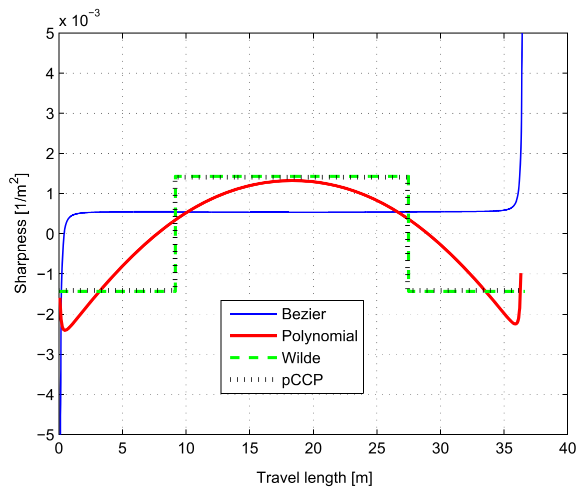

(d) Sharpness diagram

Fig. 9 ISO 3882-2 lane change paths

$\theta_i - \theta_f$ (cf. line 2 in Algorithm 2). The corresponding curvature diagrams show different path and curvature without loss of continuity, and the obtained four clothoids produce the minimal sharpness in overall length as shown in Fig. 8b.

To validate the minimal late of turning or minimal curvature variation of the proposed path, a severe lane change maneuver example (ISO 3882-2, lane width : 2.2 m, travel distance : 36.5 m) is applied with other methods in literatures of [22, 30, 31]. The path of [30] uses piecewise quadratic Bèzier curve, and the method of [31] employs quintic polynomial function.

In Fig. 9, all the paths are geometrically smooth and satisfy the boundary condition in (a), (b), but have different curvature/sharpness diagrams in (c), (d). At first, the Bèzier path have the steepest changes at both boundary for its curvature and sharpness. The polynomial path shows smooth and small curvature, but high sharpness at both boundaries. The proposed **pCCP**

Table 1 Paths comparison

Method	κ_{min}	κ_{max}	α_{min}	α_{max}
Bèzier	−0.0095	0.0297	−0.2638	1.3210
Polynomial	−0.0093	0.0097	−0.0024	0.0013
Wilde	−0.0131	0.0131	−0.0014	0.0014
pCCP	**−0.0129**	**0.0129**	**−0.0014**	**0.0014**

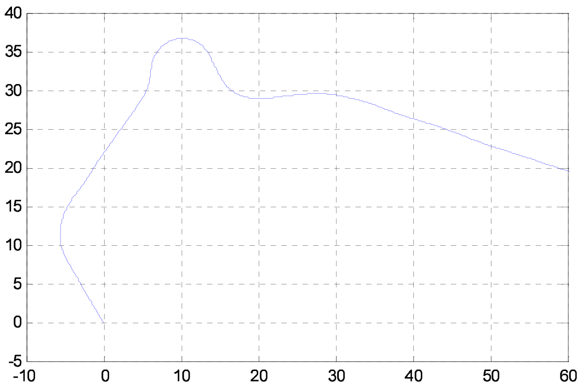

(a) Raw data path $[m]$

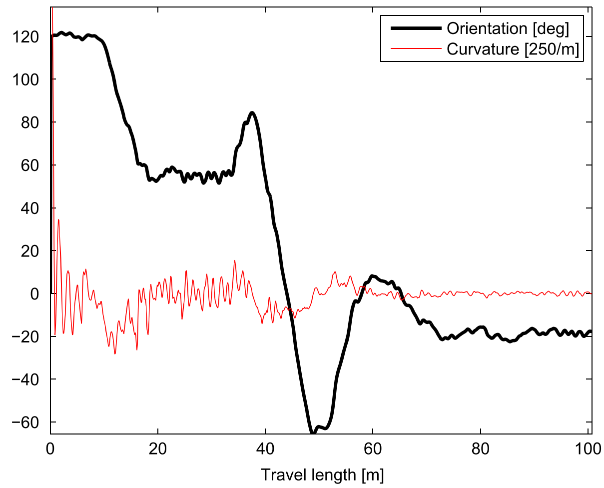

(b) Orientation$[deg]$/curvature $[1/m]$

Fig. 10 Path analysis for raw data

and *Wilde* path record almost same results, where *Wilde* path employs approximation function for the minimal amount of steering and the least maximum curvature [22], thus the obtained path has also the same characteristics as *Wilde* path.

Table 1 summarizes the comparisonal results for the lane change methods. For curvatures maximal or minimal values, the polynomial path shows the better performance, however the *Wilde* and **pCCP** record the least α_{min} value which reduces the rate of turning and exerts minimal jerk to the vehicle passenger. Even if the proposed path does not hold superior performance in minimizing the κ_{min} (or maximizing the κ_{max}), the curvature diagram shows simple and linear shape, thus easily drivable and efficient for an autonomous vehicle to follow. The results given in Fig. 9 and Table 1 also prove that the **pCCP** provides smooth and easily drivable path with minimum discomfort as *Wilde* path, while maintaining the solution generality of covering various boundary configurations as *Dubins* or *FS* paths.

5.2 Global Path Smoothing and Path Following

For car-like vehicle navigation, a smooth path is necessary so that the frequent changes in steering or jerking do not increase undesirable noises and vibration or passenger discomfort, which also causes some danger at high speed or high road curvature. In the proposed work, the smooth path generated by continuous curvatures is applied to generate a global path. One of the performances to be evaluated is to smooth the real data acquired from the vehicle driving record and to use it with a standard controller for comparative purposes. In this respect, the data is acquired from the DGPS with positional accuracy less than $2cm$ on a robotic vehicle in **PAVIN** [32]. Indeed, in the presented simulation, the vehicle is controlled to maintain a constant velocity of $1m/s$. This relatively small value has been chosen mainly to minimize the vehicle's undesirable dynamics effects.[5] In fact, the used control law [23] does not take into account the dynamic effects, only the kinematics modelling of the vehicle is used for its synthesizes. Furthermore, it is important to say that this simulation is performed in order to confirm first the viability of the proposed **pCCP** embedded in an overall autonomous navigation scheme (planning/control), and secondly as a mean to observe the advantages of the used **pCCP** as global planner. More simulations and actual experiments will be performed in near future in order to evaluate exhaustively the different paper proposals.

Even if the real data looks geometrically smooth in real scale, its analysis of orientation and curvature involves some noisy fluctuations due to sensor errors.

[5] Those effects are caused from road surface unevenness, mechanical vibration, tyre slip on the ground, and so on. It is important to also precise that when the vehicle takes tight curves with high velocity, several dynamic effects becomes important (such as the effect of Coriolis force for instance).

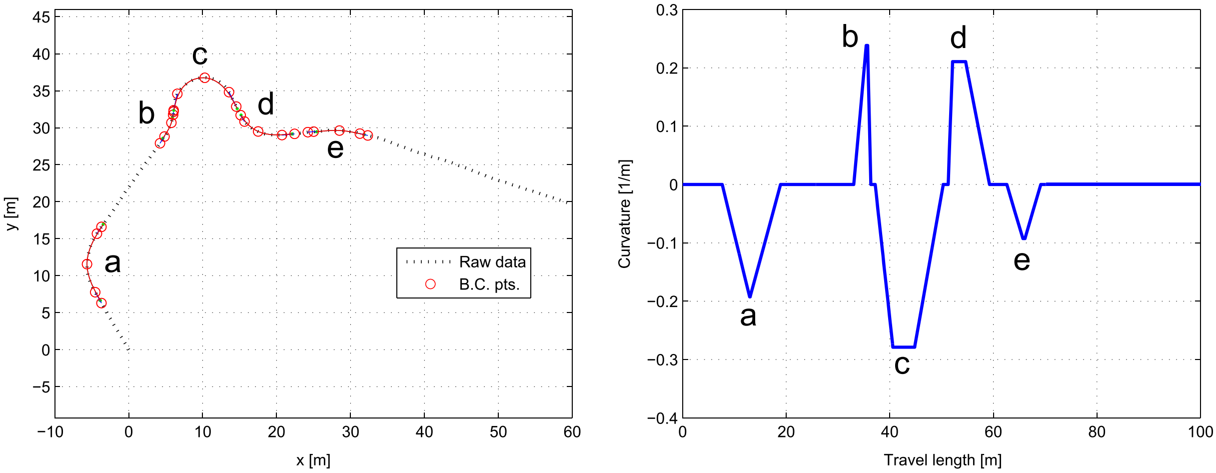

(a) Boundary conditions (b) Curvature diagram of **pCCP**

Fig. 11 Global path generation using **pCCP**

Focusing on this raw data, smoothed path generation is carried out using the proposed solution, which should have continuous curvature while reconstructing, as close as possible, the original path. From the raw data acquired, the boundary conditions are set to formulate several local path generation problems. To set the boundary conditions, pre-procedures are performed by extracting linear sections from *Hough* line/circle transform with optimization [33] (Fig. 10).

Figure 11a depicts the results of the procedure which formulate several boundary conditions and (b) shows the resultant curvature diagram for the obtained **pCCP** where each **pCCP** is solved for each boundary condition set as from **a** to **e** sections marked in Fig. 11a. The corresponding curvature diagram validates its continuity along the travel length from **a** to **e** sections with intermediate linear sections as well as simple shape compared to the noisy shape of the raw data in Fig. 10b.

The obtained **pCCP** was applied for autonomous vehicle navigation using an appropriate *Lyapunov*-based controller [23] in the global framework described in Section 1. The proposed algorithmic solution has been tested using the *Lyapunov*-based controller for

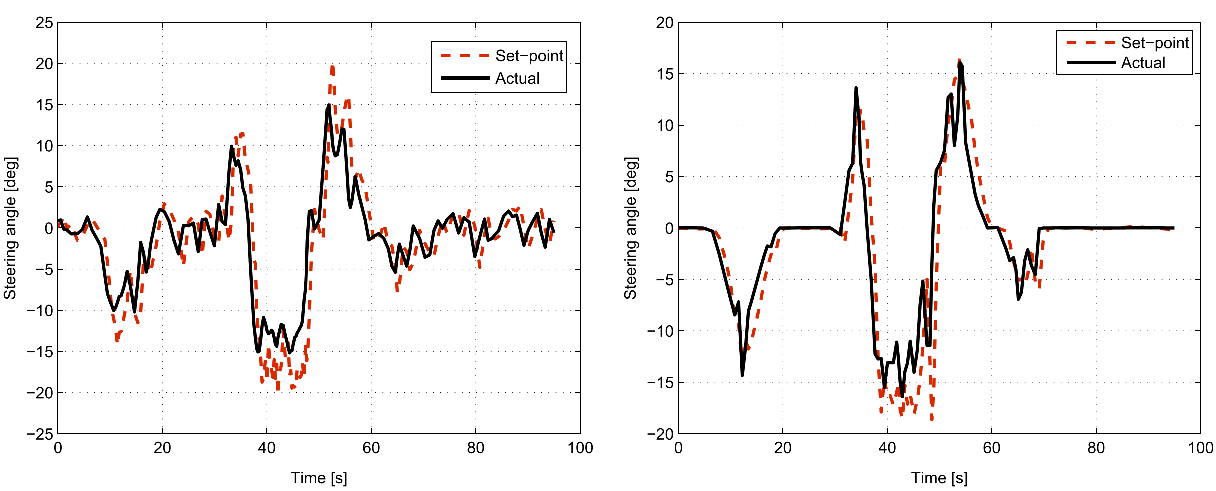

(a) Steering control for raw data (b) Steering control for obtained path

Fig. 12 Comparison of steering control with/without the proposed **pCCP**

Table 2 Performance comparison

Performance	p^e_{max}	p^e_{avg}	θ^e_{max}	θ^e_{avg}	$\lvert\kappa_{max}\rvert$	$\int\lvert\kappa\rvert\,ds$	$\lvert\alpha\rvert_{max}$	$\lvert\alpha\rvert_{avg}$
Raw Data (a)	0.027	0.007	0.087	0.020	15.184	974.606	23.461	4.652
pCCP (b)	0.028	0.003	0.068	0.012	17.349	574.852	16.317	2.491
$\frac{a-b}{a}$ [%]	−2.6	54.4	21.7	42.6	−14.3	41.0	30.5	46.5

comparing its performance with the control using raw data generated by DGPS.

Figure 12 depicts the comparisonal results of the steering set-points and atual steering angle for the two paths, where the actual steering angle is controlled to follow each path by the given controller. Figure 12a and (b) explicitly show that the actual vehicle steering has better performances to follow the set-point defined according to the proposed **pCCP**. In fact, less steering fluctuations are observed over the travel time which implies better smoothness of the actual vehicle steering. The qualitative items for these preformance are listed by $|\kappa_{max}|$ and $\int|\kappa|\,ds$ and compared on Table 2.

Figure 13 show another comparisonal result for path following performance by deviation errors of lateral distance and orientation. It is clear that according to the results shown in Fig. 13, the used **pCCP** shows better performances, highlighted with reduced lateral and orientation errors w.r.t. to the followed path. More details about the features of the obtained **pCCP** are summarized in Table 2.

In Table 2, the performances are evaluated using quantitative and qualitative measures such that the peak values (max) evaluates the quality of each path, and integrating or average (avg) values illustrate the quantitative level to analyze the performance in a synthetical manner. The maximum and average lateral position errors are denoted by p^e_{max} and p^e_{avg}, respectively, in $[m]$. It is also noted for orientation error θ^e_{max}, θ^e_{avg} in [°] and absolute sharpness by α_{max} and α_{avg} and for the maximal absolute steering κ_{max} in $[\frac{1}{m}]$ respectively.

The sharpness terms α_{max} and α_{avg} result in 30.5% and 46.5% improvement, respectively, with respect to the raw data, and these verify that the obtained steering behavior using the global **pCCP** is much smoother than the case using raw data. The remarkable difference is also shown in the total steering work through the path $\int|\kappa|\,ds$. The steering work is reduced by 41.0% compared to the driving based on the raw data. This shows that the **pCCP** algorithm generates an energy-saving trajectory for the vehicle using smooth and continuous steering. Only deteriorated results on the lateral and orientation errors are found at the time around $47sec$ in Fig. 13 which corresponds to the section **c** in Fig. 11. This deviation is caused from the long circular section of **c** in the original path where

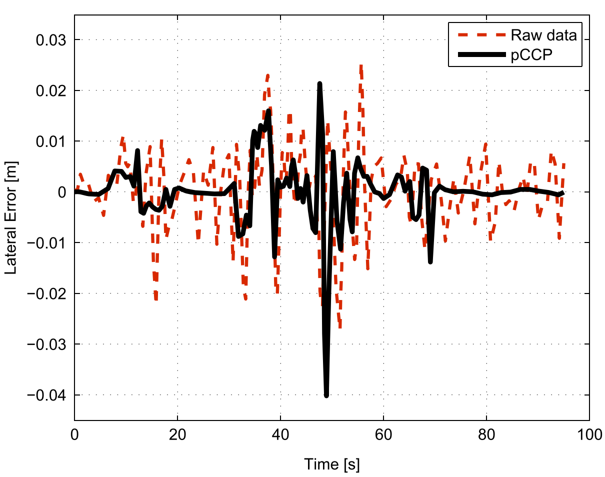

(a) Lateral errors

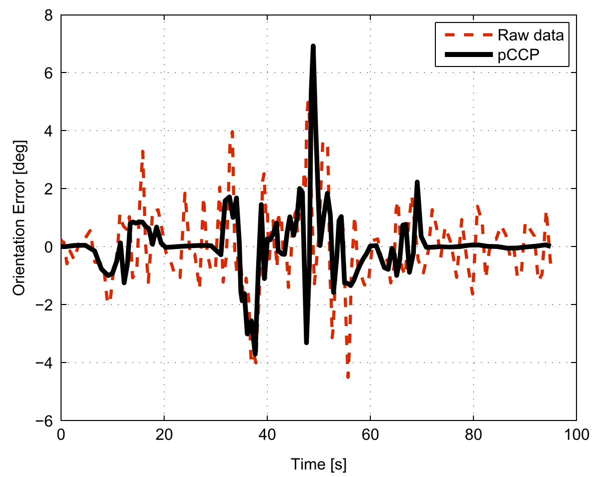

(b) Orientation errors

Fig. 13 Path following performances with/without the proposed **pCCP**

the proposed path is not optimized to fit for the overall circular segment, and the proposed algorithm is required to be improved for regenerating closeness to those sections.

Results given in Fig. 12, Fig. 13 and Table 2 demonstrate that the smoothed path determined by clothoid segments provides an enhanced performance for the path driven by a nonholonomic car-like vehicle. The reduced steering work and sharpness decreases, enhance therefore the passenger comfort by reducing the lateral acceleration and vehicle jerk [18].

With regard to the algorithmic performance, every clothoid generation takes less than $5ms$ when using an Intel Celeron CPU with $1.50GHz$ in a MATLAB® environment. The number of iterations for algorithmic convergence is $8 \sim 10$ loops for achieving the solution within the convergence threshold $D_e = 10^{-2}m$.

6 Conclusion

This paper addressed continuous curvature path problems and proposed an *algorithmic* methodology to generate clothoid-based **pCCP** using parametric adjustment. A defined problem for car-like vehicle path generation is classified into two cases, where each problem is formulated according to the geometrical relation between initial and final configurations. For algorithmic efficiency, the minimax sharpness constraint is proposed with empirically fitted initial parameter assumptions. The algorithmic procedure obtains pCCP for each problem while ensuring efficient convergence. The usefulness of the proposed solutions are *reinforced* by some demonstrative examples applied to both local path planning and global path regeneration schemes. The obtained overall vehicle path based on **pCCP** showed its high potentiality and interest to be implemented in an actual autonomous navigation software with more precise map by detailed information of steering guidance as well as its control.

In future work, the performance of the proposed algorithmic methodology will be tested with an actual experimental vehicle while considering uncertain errors, such as motor actuation dynamics and/or the nonlinear tire contact dynamics on the road surface. Therefore, to enhance further the features of the obtained vehicle navigation, several elements, dealing mainly with modelling and data uncertainties, are targeted to be taken into account, among them let us cite: the use of more robust control (for environment, input/output unmodelled dynamics or perception/actuation) permitting to link the steering guidance set-points to its actual vehicle navigation behavior. This could be done while accurately identifying steering nonlinearities of the mechanical/electrical vehicle components in order to take them into consideration in the planning/control phases. This identification could be done either while using experimental calibrations or considering an automatic tuning process from a large amount of experimental database. It is also planned to reduce/eliminate the ground unevenness effects on the collected data.

Acknowledgments This research was supported, in part, by the Space R&D Program of National Research Foundation (NRF), NRF-2013M1A3A3A02042335, sponsored by the Korean Ministry of Science, ICT and Planning (MSIP), in part, by the Fundamental Research Program of Korea Evaluation Institute of Industrial Technology (KEIT), 2015-10060160, sponsored by the Korean Ministry of Trade, Industry and Energy (MOTIE).

This research was also funded by the French National Research Agency (ANR) through the support of LabEx IMobS3 (ANR-7107-LABX-716701). The authors deeply appreciate to Prof. Doran K. Wilde for his proof reading and very helpful suggestions.

Appendix: Clothoid Property for Parameter Variation

From Eq. 8, following is derived.

When $s = (2\delta)^{\frac{1}{2}} \cdot \alpha^{\frac{-1}{2}}$, then $\frac{ds}{d\alpha} = \alpha^{\frac{-3}{2}} \cdot [-\delta^{\frac{1}{2}}]$. Thus, if a constant $\delta > 0$ with $\alpha > 0$, then $\frac{ds}{d\alpha} < 0$, and it is true that for an increasing α, the length s shrinks while the clothoid bends upward (cf. Fig. 1).

Other patterns of $\frac{ds}{d\kappa}$ or $\frac{ds}{d\delta}$ could be obtained by the same analogy.

References

1. Solea, R., Nunes, U.: Trajectory planning with velocity planner for fully-automated passenger vehicle. Intel. Transp. Syst. Conf. 474–480 (2006)
2. Villagra, J., Milantes, V., Perez, J., Godoy, J.: Smooth path and speed planning for an automated public transport vehicle. Robot. Auton. Syst. **60**, 252–265 (2012). doi:10.1016/j.robot.2011.11.001
3. Macek, K., Philippsen, R., Siegwart, R.: Path following for autonomous vehicle navigation based on kinodynamic control. J. Comput. Inf. Technol. **17**, 17–26 (2009)

4. Elfes, A.: Occupancy Grids : a probabilistic framework for robot perception and navigation. PhD thesis, Department of Electrical and Computer Engineering, Carneigie Mellon University (1989)
5. Khatib, O.: Real-time obstacle avoidance for manipulators and mobile robots. Int. J. Robot. Res. **5**(1), 90–98 (1986)
6. Kelly, A., Nagy, B.: Reactive nonholonomic trajectory generation via parametric optimal control. Int. J. Robot. Res. **22**(7–8), 583–601 (2003)
7. Likhachev, M., Ferguson, D.: Planning long dynamically feasible maneuvers for autonomous vehicles. Int. J. Robot. Res. **28**(8), 933–945 (2009)
8. Vilca, J., Adouane, L., Mezouar, Y.: Reactive navigation of mobile robot using elliptic trajectories and effective on-line obstacle detection. Gyroscopy and Navigation **4**(1), 14–25 (2013). Springer Verlag, Russia ISSN 2075 1087
9. Chakravarthy, A., Ghose, D.: Obstacle avoidance in a dynamic environment: A collision cone approach. IEEE Trans. Syst. Man Cybern. Syst. Hum. **28**(5), 562–574 (1998)
10. Fulgenzi, C., Spalanzani, A., Laugier, C.: Dynamic obstacle avoidance in uncertain environment combining pvos and occupancy grid. IEEE Int. Conf. Robot. Autom. 1610–1616 (2007)
11. Adouane, L.: Reactive versus cognitive vehicle navigation based on optimal local and global pelc*. Robot. Auton. Syst. **88**, 51–70 (2017)
12. Yang, K., Jung, D., Sukkarieh, S.: Continuous curvature path-smoothing algorithm using cubic bezier spiral curves for non-holonomic robots. Adv. Robot. **27**(4), 247–258 (2013)
13. Lamiraux, F., Laumond, J.P.: Smooth motion planning for car-like vehicles. IEEE Trans. Robot. Autom. **17**(4), 498–501 (2001)
14. Montes, N., Mora, M.C., Tornero, J.: Trajectory generation based on rational Bezier curves as clothoids. IEEE Intel. Vehicles Symposium 505–510 (2007)
15. Avanzini, P., Thuilot, B., Martinet, P.: Manual convoying of automated urban vehicles relying on monocular vision. Int. Vehicles Symposium 19–24 (2012)
16. Dubins, L.E.: On curves of minimal length with a constraint on average curvature, and with prescribed initial and terminal positions and tangents. Am. J. Math. **79**, 497–516 (1957)
17. Reeds, J.A., Shepp, L.A.: Optimal paths for a car that goes both forwards and backwards. Pac. J. Math. **145**(2), 367–393 (1990)
18. Labakhua, L., Nunes, U., Rodrigues, R., Leite, F.S.: Smooth trajectory planning for fully automated passengers vehicles: spline and clothoid based methods and its simulation. In: A.C. et al. (ed.) Informatics in Control Automation and Robotics, Volume 15 of Lecture Notes Electrical Engineering, pp. 159–182 (2008). doi:10.1007/978-3-540-79142-3-14
19. Fraichard, T., Scheuer, A.: From Reeds and Shepp's to continuous curvature paths. IEEE Trans. Robot. **20**, 1025–1035 (2004)
20. Parlangeli, G., Indiveri, G.: Dubins inspired 2d smooth paths with bounded curvature and curvature derivative. In: Proceedings of the 7th IFAC Symposium on Intelligent Autonomous Vehicles, pp. 252–257 (2010)
21. Walton, D.J., Meek, D.S.: A controlled clothoid spline. Comput. Graph. **29**, 353–363 (2005)
22. Wilde, D.K.: Computing clothoid segments for trajectory generation. IEEE/RSJ International Conference on Intelligence Robots and Systems, pp. 2440–2445 (2009)
23. Canudas, C., Sicliano, B., Bastin, G.: Theory of robot control. Springer, Berlin Heidelberg, ISBN 3-540-76054-7 (1996)
24. DeLuca, A., Oriolo, G., Samson, C.: Feedback control of a nonholonoic car-like robot (Robot Motion Planning and Control). Springer, Berlin Heidelberg (1998)
25. Adouane, L.: An adaptive multi-controller architecture for mobile robot navigation. In: 10th IAS, Intelligent Autonomous Systems, Baden-Baden, Germany, pp. 342–347 (2008)
26. Valipour, M.: Sprinkle and trickle irrigation system design using tapered pipes for pressure loss adjusting. J. Agric. Sci. **4**(12), 125–133 (2012)
27. Valipour, M.: Comparison of surface irrigation simmulation models: full hydrodynamic, zero inertia, kinematic wave. J. Agric. Sci. **4**(12), 68–74 (2012)
28. Valipour, M., Banilhabib, M.E., Behbahani, S.M.R.: Comparison of the arma, arima, and the autoregressive artificial neural network models in forecasting the monthly inflow of dez dam reservoir. J. Hydrol. **476**(7), 433–441 (2013)
29. Kiusalaas, J.: Numerical methods in engineering with MATLAB. Cambridge University Press UK, Shaftesbury Road, Cambridge CB2 8BS, UK (2007)
30. Chen, J., Zhao, P., Mei, T., Liang, H.: Lane change path planning based on piecewise bezier curve for autonomous vehicle. In: IEEE International Conference on Vehicular Electronics and Safety, pp. 17–22 (2013)
31. Wang, Y., Cartmell, M.P.: Trajectory generation for a four wheel steering tractor-trailer system: a two-step method. Robotica 16(4)
32. Vilca, J.M., Adouane, L., Mezouar, Y.: A novel safe and flexible control strategy based on target reaching for the navigation of urban vehicles. Robot. Auton. Syst. **70**, 215–226 (2015)
33. Gim, S., Adouane, L., Lee, S., Derutin, J.P.: Parametric continuous curvature trajectory for smooth steering of the car-like vehicle. In: International Conference on Intelligent Autonomous Systems (2014)

Suhyeon Gim majored in mechanical engineering for bachelors (2001) and masters (2003) degree in Korea University and then, acquired doctors degree in IT engineering (2009). He has worked for medical robot development at the Korean National Cancer Center, KIST and is now working in Meere-company. He has researched on the path planning algorithm for autonomous navigated vehicles by Double PhD cotutorship program of SungKyunKwan University and University Blaise Pascal since 2011.

Lounis Adouane is an Associate Professor since 2006 at the Institut PascalPolytech Clermont-Ferrand in France. He received anMS in 2001 from IRCCyN-ECN Nantes, where he worked on the control of legged mobile robotics. In 2005, he obtained a Ph.D. in automatic control from FEMTO-ST laboratory-UFC Besancon. During his Ph.D. studies he deeply investigated the field of multi-robot systems, especially those related to bottom-up and reactive control architec-tures. After that, he joined in 2005 Ampre laboratory-INSA Lyon and studied hybrid (continuous/discrete) control architectures applied to cooperative mobile robot arms. Dr. Adouane had the opportunity to visit several institutions/laboratories, such as 1 month in 2009 at LIST (Luxembourg) and 6 months in 2014 at Cranfield and Kingston universities (United Kingdom). In 2015, he obtained from Blaise Pascal University a HDR (habilitation to steer research in Robotics). Since 2006, he has authored/coauthored more than 70 international references and 2 books. His main research interests include: Autonomous mobile robots/vehicles, Behavioral/multi-controller architectures, Obstacle avoidance, Lyapunov-based synthesis and stability, Cooperative robotics, Task/trajectory planning and re-planning, Artificial intelligence, Multi-robot/agent simulation.

Sukhan Lee is currently Distinguished Chair Professor and Founding Direc-tor of the Intelligent Systems Research Institute at Sungkyunkwan University. He is also serving as a Vice President of Korea National Academy of Science and Technology. He served as Dean of the University Graduate Studies from 2011 to 2013, WCU Professor of Interaction Science from 2008 to 2013 and Professor of Information and Communication Engineering from 2003 to 2014. From 1998 to 2003, he was with the Samsung Advanced Institute of Technology as an Executive Vice President and a Chief Research Officer. From 1990 to 1997, he worked for Jet Propulsion Laboratory/NASA, California Institute of Technology, as a Senior Member of Technical Staff. From 1983 to 1997, he was with the Department of Electrical Engineering and Computer Science at the University of Southern California as a Professor. Prof. Sukhan Lee received his Ph.D. degree in Electrical Engineering from Purdue University, West Lafayette, and his M.S. and B.S. degrees in Electrical Engineering from Seoul National University. Prof. Sukhan Lee is a life fellow of IEEE and a fellow of Korean National Academy of Science and Technology. He served as a Vice President of IEEE Robotics and Automation Society from 2004-2008. He has published over 400 technical papers in Scientific Journals and Major Conferences, over 90 Domestic/International Patents and 6/35 Books/Book Chapters. He has his research interest in robotics, computer vision and artificial intelligence.

Jean-Pierre Dérutin is currently a full professor at PolytechClermont-Blaise Pascal University since 1994. Pr Drutin is also leader of the Image, Perception Systems, Robotic (IPSR) research group from the Pascal Institut - UMR 6602. He received his Ph.D. in Computer Science from the Blaise Pascal University (INPT) for his work on real-time image processing system in 1982. He obtains the grade of Professor in 1994. Pr Derutin research interests focus on two major axes: intelligent transportation systems and smart sensors. These themes deal with the artificial perception from the sensor up to the representation at the highest level of the environment along with the elaboration of the particular architectures that it implicates. The ambition of this wide theme is to develop global perception approaches using sensors in view of comprehending the environment and to adapt them next to the sensors according to optimized methodologies in terms of performance, system and embedded possibilities.